Polarization transfer in ion-surface scattering

Winters, Danyal Ferdinant Alexander

Chapter 2

Ion-surface fundamentals

2.1 Introduction

The main purpose of this chapter is to give an overview of the ion-surface processes of relevance for the experiments presented in this thesis. The reason for this approach is that the ion-surface interaction is a very complex, dynamical many-body problem. This is in particular true for Multiply Charged Ions (MCI's) impinging on surfaces. A rigorous theoretical description of the ion-surface interaction is beyond the scope of this thesis. The discussion is also limited to surfaces of conducting targets.

The ion-surface interaction is mostly treated in terms of a combination of classical and quantum mechanics. The projectile trajectory is treated classically and is described by trajectory-changing binary projectile-target atom collisions using Monte Carlo techniques. A well-known and often used code is MARLOWE [37, 38]. Electronic interactions between ion and surface are mostly treated quantum mechanically. The target electrons are usually described as a non-interacting free Fermi gas. Projectile electron orbitals are described by hydrogenic wave functions. The electronic exchange interaction between ion and surface is treated in terms of overlap between the target states and the projectile states.

In the early fifties, Hagstrum [39] performed experiments on Auger ejection of electrons from metals by ions. After his pioneering work the field has grown strongly. Many types of experiments, covering a wide range of ion-surface combinations, have been performed. For an overview see *e.g.* Arnau *et al* [13] and Winter [14]. However, because of the above mentioned complexity, there are still many questions that remain to be answered, especially concerning the dynamic neutralization of MCI's in front of a surface (this thesis).

In section 2.2, the most widely used neutralization model, the Classical Over

the Barrier (COB) model, will be outlined. The over-the-barrier approach was originally developed for describing electron capture by MCI's colliding on atoms [40, 41, 42]. Later, the COB model was modified to describe the neutralization of MCI's in front of metal surfaces [43, 44].

Section 2.3 deals with reaction processes which can occur due to the ion-surface interaction. Autoionization (section 2.3.5) and radiative decay (section 2.3.6) are throughout this thesis the most important processes.

Atomic units (a.u.), $\hbar = 1$, $e = 1$ and $m_e = 1$, will be used throughout this thesis. See Appendix 1 for an overview of the values of the atomic units.

2.2 Classical over the barrier model

Conceptually, the COB model for neutralization of an ion (projectile) in front of a conducting surface (target) is very simple: an electron will be exchanged between target and projectile when the 'classical' electrostatic potential between them is low enough to allow for resonant transfer of the electron 'over the barrier'. According to the COB model, on the way towards the surface the ion is neutralized *stepwise* by successive electron capture. The potential barrier between ion and surface, experienced by an electron $-e$, is formed by the combined potential of the ion with charge state $+q$ and the potentials of the *image charges* of the ion $-q$ and the electron $+e$. This is illustrated in figure 2.1.

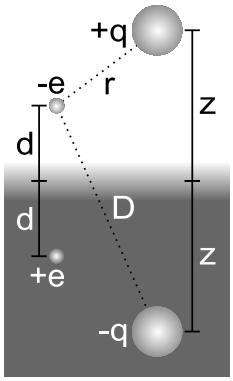

Figure 2.1: Illustration of the image charges.

These image charges are deduced from the following: When an ion approaches the surface, free electrons in the target are attracted by the electrostatic force (between projectile and target) towards the surface. The attracted electrons bundle into an electron cloud that 'screens' the surface from the incoming charge. In the adiabatic limit, *i.e.* when the projectile velocity v_i is

much smaller than the Fermi velocity v_F of the target electrons, the screening effect of the electron cloud can be described in terms of a classical electrostatic image potential V_t.

The description in terms of images requires the existence of an image plane close to the surface. The surface is usually defined as the point where the target electron density has dropped to half of its original value, *i.e.* the 'jellium edge'. The jellium edge is usually situated about half an atomic layer above the topmost atomic layer. The image plane does not exactly coincide with the jellium edge ($z = 0$) but lies (mostly) just slightly outside the jellium surface ($z > 0$) [45]. For our purposes the difference is negligible and therefore we take $z = 0$ as the position of the image plane (surface).

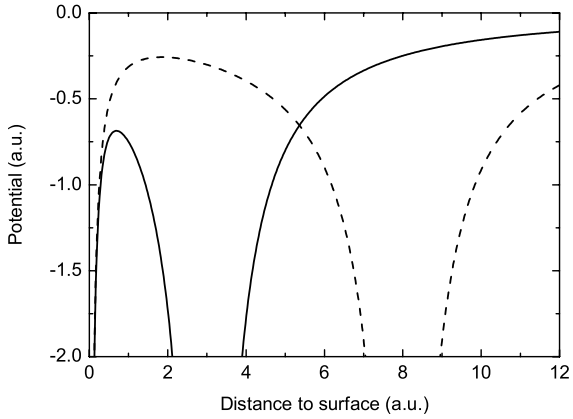

Figure 2.2: The electron potential V_t versus distance d above the surface for a doubly charged ion at 3 and 8 a.u. distance from the surface.

The total potential V_t experienced by the electron at position d in front of the surface is the sum of the ion potential (at $+z$), the ion image potential (at $-z$) and the self-image potential of the electron (at $-d$). Assuming the electron to be positioned on the ion-surface axis and using the substitutions $r = z - d$ and $D = z + d$, one obtains for the 1D potential

$$V_t = -\frac{q}{z-d} + \frac{q}{z+d} - \frac{1}{4d} \tag{2.1}$$

Figure 2.2 shows the total potential V_t, for a projectile in charge state $q = 2$, when the ion is located at $z = 8$ a.u. (dashed line) and at $z = 3$ a.u. (solid line) in front of the surface. Negative distances correspond to penetration into the target. From fig. 2.2 it can be seen that the potential barrier is lowered as the ion comes closer to the surface.

The critical distance z_0 at which the COB neutralization sequence starts can be estimated as follows. Classically, the position z_0 is reached when the saddle point V_s of the total potential V_t (located between the projectile and target) is lowered and becomes equal to the work function ϕ of the surface. Then surface electrons at the Fermi level, *i.e.* the least bound electrons, can resonantly transit over-the-barrier.

The position of the saddle point is found by equating the partial derivative of the potential to zero, *i.e.* $\partial V_t/\partial d = 0$. To a very good approximation, the position of the saddle point is then given by [43]

$$d_s = \frac{z}{\sqrt{8q+2}} \approx \frac{z}{\sqrt{8q}} \tag{2.2}$$

Note that the position of the saddle point only depends on the position z and the charge state q of the incoming projectile. Inserting d_s into equation (2.1), one finds for the saddle point potential

$$V_s = -\frac{\sqrt{8q+2}(16q+1)}{4z(8q+1)} \approx -\frac{\sqrt{2q}}{z} \tag{2.3}$$

Equating V_s to the work function ϕ of the surface, gives the neutralization distance z_0 for COB neutralization [43]

$$z_0 = \frac{\sqrt{8q+2}}{2\phi} \approx \frac{\sqrt{2q}}{\phi} \tag{2.4}$$

The principal quantum number n of the state into which first neutralization takes place, can be calculated in a hydrogenic approximation and is found to be [13]

$$n = \frac{q}{\sqrt{2\phi}}\left(1+\frac{q-1/2}{\sqrt{8q}}\right)^{-1/2} \approx \frac{q}{2\sqrt{\phi}} \tag{2.5}$$

One of the prominent effects of the image interaction - especially for MCI's - is the acceleration of the ion towards the surface. This yields an upper bound on the time the ion can spend in front of the surface. The classical image force experienced by an ion with charge state $+q$ at a distance z above the surface is given by $F_{im} = -q^2/(4z^2)$. Assuming stepwise charge transfer each time the ion reaches a z_0 for which the next electron capture is classically allowed, and assuming that the captured electron completely screens one unit of charge of the incoming ion, the total image energy E_{im} gained by the projectile until complete neutralization, is to a fair approximation given by [13]

$$E_{im} = \frac{q^{3/2}}{3}\frac{\phi}{\sqrt{2}} \tag{2.6}$$

Due to the image charges, the projectile states are also modified as the projectile approaches the surface. The binding energy of a projectile valence electron will decrease due to the Coulomb interaction with the image charge of its ionic core. For a valence electron, the additional charges of the self-image and the projectile image result in first order perturbation to a shift ΔE_B of the 'free atom' binding energy E_B [46]

$$\Delta E_B = \frac{2q+1}{4z} \tag{2.7}$$

As the projectile approaches the surface, Resonant Transitions (RT's) between projectile and target states can occur, see section 2.3.1, leading to the formation of an excited projectile state. The excited projectile state has a natural lifetime τ and a natural decay rate $\gamma = 1/2\tau$ [47]. The natural line width Δ_B of the excited projectile state is the FWHM of its Lorentzian intensity distribution $I(E'_B)$

$$I(E'_B) \sim \frac{1}{(E_B - E'_B)^2 + \gamma^2} \tag{2.8}$$

Where E_B and E'_B are the initial and final projectile states, respectively. From equation 2.8 it can be seen that the FWHM is 2γ, which means that the natural line width is $\Delta_B = 2\gamma = 1/\tau$. The RT's increase the decay possibilities of the excited state, *i.e.* γ is increased and the line width is broadened. Resonant transition rates increase exponentially as the projectile approaches the surface and so does the line width.

2.3 Reaction processes

The reaction processes discussed in this section can be divided into two classes: primary and secondary reaction processes. Primary processes involve charge exchange, or electron transfer, between projectile and target. The secondary processes are pure projectile related de-excitation processes. The primary reaction processes are sub-divided into four types: Resonant Transitions (RT), Collective Excitations (CE), Auger Neutralization (AN) and Auger De-excitation (AD). The secondary reaction processes are sub-divided into two types: AutoIonization (AI) and Radiative Decay (RD). The primary reaction processes will be discussed first. Then, the secondary processes will be treated in some more detail.

2.3.1 Resonant transitions

One or more electrons are resonantly exchanged between target and projectile. There is no excess energy and no electrons are emitted. In figure 2.3, a plot of

the binding energy E_B versus the distance to the surface, the RT's schematically indicated. The target (solid) density of states is shown on the left side of the abscissa, the discrete projectile (ion) states on the right. There are two types of over-the-barrier RT's: Resonant Neutralization (RN), in which the projectile is neutralized by target electrons, and Resonant Ionization (RI), in which the projectile is ionized by losing electrons to the target. Also shown is Quasi Resonant Neutralization (QRN), in which the projectile is neutralized by 'quasi resonant' tunneling of target electrons through the potential barrier. Especially for MCI's, the RT's already occur at large distances above the surface because of the low potential barrier for high charge states. Therefore, certainly in the initial stages of the interaction, tunneling processes play only a minor role and can be neglected.

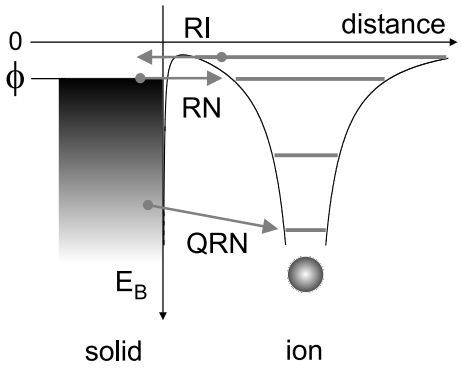

Figure 2.3: Resonant transitions.

The rate Γ_{RT} with which an electron can be exchanged between target and projectile $+q$, located a distance z in front of the surface, is to first order given by Fermi's golden rule (see *e.g.* [39, 35])

$$\Gamma_{RT} = 2\pi \left|H_{fi}\right|^2 \rho_f \tag{2.9}$$

Here, ρ_f is the density of final states and H_{fi} is the coupling between the final (projectile) state $|\psi_f\rangle$ and the initial (target) state $|\psi_i\rangle$. The density of the final projectile states is completely specified, therefore ρ_f is equal to the Density Of States (DOS) of the target at an energy resonant with the projectile energy level. The coupling between the final and initial state is given by the matrix element

$$H_{fi} = \left\langle \psi_f \left| -\frac{q}{r} \right| \psi_i \right\rangle \tag{2.10}$$

The potential centered between the brackets is the attractive Coulomb potential of the projectile nucleus. The electron is located a distance r from the projectile center. Since the final and initial wave functions decay exponentially with

increasing z, so does the matrix element H_{fi}. The rate Γ_{RT} will therefore also decay exponentially for large z, *i.e.*

$$\Gamma_{RT}(z) = \Gamma_{RT}(0)e^{-\alpha_{RT}z} \tag{2.11}$$

The maximum rate $\Gamma_{RT}(0)$ is obtained at $z = 0$. The factor α_{RT} is the inverse decay length of the coupling matrix element H_{fi}. Resonant transition rates $\Gamma_{RT}(0)$ are typically in the range between 0.01 and 0.1 atomic units, which is about $\sim 10^{15}$ Hz (see chapter 6).

2.3.2 Collective excitations

A target electron is captured into a more strongly bound projectile state, the excess energy is stored into the target electronic structure causing an excitation involving many electrons, called a *plasmon* [48]. No electrons are emitted during or after this reaction process. Figure 2.4 schematically shows the Collective Excitation (CE). Collective excitations can be recognized as 'dips' in the energy distribution of target electrons emitted during ion bombardment [49]. Bulk plasmons can be distinguish from surface plasmons by differences in energy, *e.g.* for Al $\hbar\omega_b \sim 15$ eV and $\hbar\omega_s \sim 10$ eV [49].

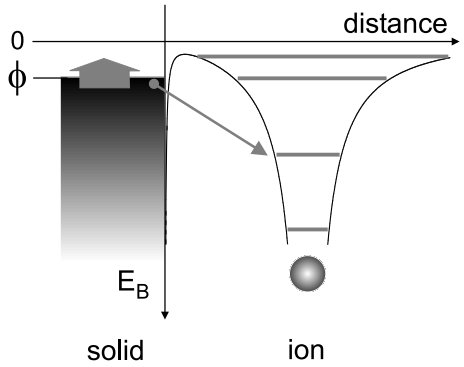

Figure 2.4: Collective excitations.

2.3.3 Auger neutralization

A target electron is captured into a more strongly bound projectile state, the excess energy is used to eject an electron from the target into the vacuum. Figure 2.5 schematically shows the Auger Neutralization (RN) process. The maximum kinetic energy E_k of the Auger electron emitted from the target is $E_k = E_B - 2\phi$. Here, E_B is the binding energy of the projectile level and ϕ is the work function. In this case both electrons originate from the top of the (solid)

valence band, *i.e.* the Fermi level, maximizing the energy difference between target and projectile level. The width ΔE_k is given by the self-convolution of the Surface Density of States (SDOS).

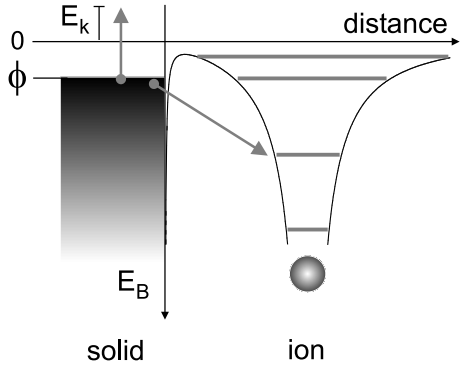

Figure 2.5: Auger neutralization.

The AN rates depend like RT's on the coupling between final (projectile) state $|\psi_f\rangle$ and initial (target) state $|\psi_i\rangle$, but the coupling matrix element H_{fi} is now determined by the repulsive electron-electron interaction. Like in the case of the RT's, at least for large z, the AN rate also decays exponentially with increasing z

$$\Gamma_{AN}(z) = \Gamma_{AN}(0)e^{-\alpha_{AN}z} \tag{2.12}$$

For small z the structure of the wave functions has to be taken into account. The decay rate depends on the inverse decay length α_{AN} and has a maximum value of $\Gamma_{AN}(0)$. Typical AN rates $\Gamma_{AN}(0)$ are in the range between 0.01 and 0.5 a.u. [50].

2.3.4 Auger de-excitation

A surface electron is captured into a more strongly bound projectile state, the excess energy is used to eject a less strongly bound projectile electron into the vacuum. The AD process is depicted in figure 2.6. The maximum energy of the Auger electron emitted from the projectile is $E_k = E_B - \phi - E'_B$, where E_B and E'_B are the binding energies of the more strongly bound and the less strongly bound projectile levels, respectively. Like in the case of AN, the width ΔE_k reflects the SDOS and the final and initial states involve projectile and target, respectively. Therefore the AD process is comparable to the AN process and the rates $\Gamma_{RD}(0)$ range between 0.01 and 0.5 a.u..

The secondary reaction processes, radiative decay and autoionization of excited projectile states, will now be discussed. These processes typically occur

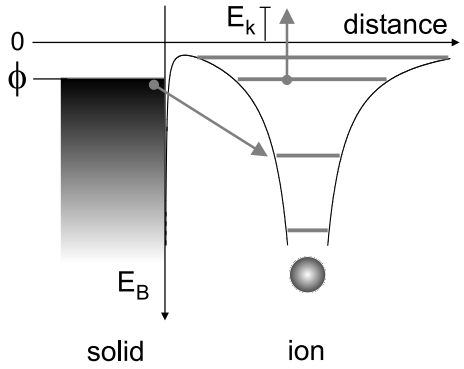

Figure 2.6: Auger de-excitation.

after a primary charge exchange process between target and projectile. Both processes are of importance in the discussion on the spin-polarized surfaces (chapter 5), since two spectroscopic techniques, AES and ECS, based on these processes are employed to study spin ordering effects.

2.3.5 Autoionization

Of all reaction processes discussed so far, for the work presented in this thesis AutoIonization (AI) [51] is one of the most important process, since it will be employed to study spin-polarized surfaces (chapter 5). The AI process is schematically shown in figure 2.7. An excited projectile, *e.g.* a MCI neutralized via RN, decays under the emission of a projectile electron into the vacuum. The kinetic energy of the emitted electron - the Auger electron - is given by $E_k = E_B - E'_B$, *i.e.* the difference in total binding energy between the initial E_B and the final E'_B states.

The AI decay rate Γ_{AI} is given by Fermi's Golden rule. The density of final states ρ_f is now purely atomic and thus well-defined

$$\Gamma_{AI} = 2\pi \left|H_{fi}\right|^2 \rho_f \tag{2.13}$$

The coupling H_{fi} between the final $|\psi_f(1,2)\rangle$ and initial $|\psi_i(1,2)\rangle$ atomic states is given by the matrix element

$$H_{fi} = \left\langle \psi_f(1,2) \left| \frac{1}{|\vec{r}_1 - \vec{r}_2|} \right| \psi_i(1,2) \right\rangle \tag{2.14}$$

The potential centered between the brackets is the repulsive electron-electron potential. Autoionization is an intra-atomic process and therefore Γ_{AI} does not depend on the distance to the surface. In general, AI rates depend only

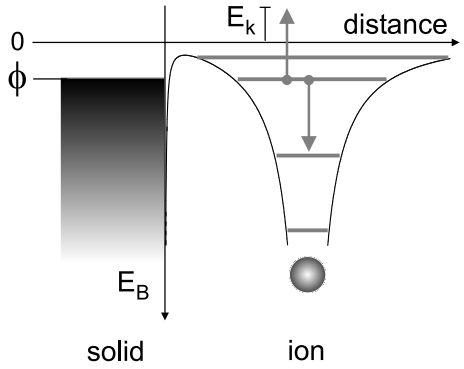

Figure 2.7: Autoionization.

weakly on the nuclear charge Z of the projectile and in light elements this is the dominant decay process. There exists atomic structure software which allows for *ab initio* calculations of AI decay rates [52]. AI transition rates Γ_{AI} are, depending on the states involved, in the range between 0.001 to 0.01 a.u., which is about 10^{14} Hz (see chapter 6 and *e.g.* [43]).

Since the initial and final projectile states are well-defined, so is the energy of the Auger electron. The energy resolution ΔE_k with which the energy distribution $I(E_k)$ of the Auger electrons can be measured is therefore experimentally limited. The spectroscopic technique used to obtain $I(E_k)$ is called Auger Electron Spectroscopy (AES) and the measured distribution is also called an 'Auger spectrum'. High resolution electrostatic analyzers (section 3.3.2) can resolve the fine structure of the projectile states. Hence, it is possible to measure the population of the individual projectile states during the ion-surface interaction. In turn, this can provide important information on the neutralization dynamics and on *e.g.* the spin polarization of the target electrons (chapter 5).

2.3.6 Radiative decay

An excited projectile can decay to a stronger bound state by the emission of a photon. The wavelength of the emitted radiation is given by $\lambda = hc/(E_B - E'_B)$, where E_B and E'_B are the initial and final state binding energies, respectively. The Radiative Decay (RD) process is shown in figure 2.8. Photon emission rates Γ_P increase rapidly with increasing nuclear charge Z, for hydrogen-like wave functions even as fast as Z^4. RD is thus not very likely to occur in light elements but becomes more likely for the heavier elements. Typical rates for hydrogenic ions are given by $\Gamma_P \simeq 4 \cdot 10^{-7} Z^4/n^{4.5}$ [53].

As mentioned above, the RD process is also used to study spin-polarized

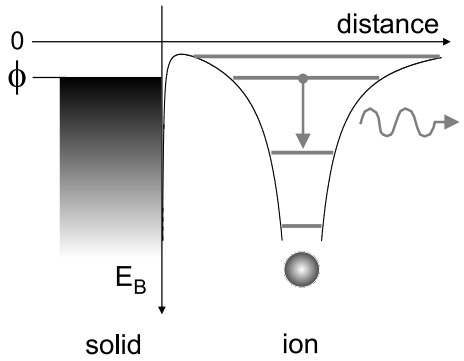

Figure 2.8: Radiative decay.

surfaces. By analysis of the degree of polarization of the fluorescence of the decaying excited projectile states E_B, information on the electron distribution over the available projectile states can be obtained (chapter 5).